Acta Crystallographica Section D
Biological Crystallography
ISSN 0907-4449

Structures of pseudechetoxin and pseudecin, two snake-venom cysteine-rich secretory proteins that target cyclic nucleotide-gated ion channels: implications for movement of the C-terminal cysteine-rich domain

Nobuhiro Suzuki,[a,b]‡§ Yasuo Yamazaki,[c]§ R. Lane Brown,[d] Zui Fujimoto,[b] Takashi Morita[c]* and Hiroshi Mizuno[b,e,f]*

[a]Department of Applied Biochemistry, University of Tsukuba, Tsukuba, Ibaraki 305-8572, Japan, [b]Department of Biochemistry, National Institute of Agrobiological Sciences, Tsukuba, Ibaraki 305-8602, Japan, [c]Department of Biochemistry, Meiji Pharmaceutical University, Kiyose, Tokyo 204-8588, Japan, [d]Neurological Science Institute, Oregon Health and Science University, Beaverton, Oregon 97006, USA, [e]VALWAY Technology Center, NEC Soft Ltd, Koto-ku, Tokyo 136-8627, Japan, and [f]Institute for Biological Resources and Functions, National Institute of Advanced Industrial Science and Technology, Central 6, Tsukuba, Ibaraki 305-8566, Japan

‡ Present address: Structural Biology Research Center, Institute of Materials Structure Science, High Energy Accelerator Research Organization (KEK), Tsukuba, Ibaraki 305-0801, Japan.
§ These authors contributed equally to this work.

Correspondence e-mail: tmorita@my-pharm.ac.jp, mizuno-hiroshi@aist.go.jp

Received 1 May 2008
Accepted 25 July 2008

PDB References: pseudechetoxin, 2dda, r2ddasf; pseudecin, 2ddb, r2ddbsf; pseudecin, Zn^{2+} bound, 2epf, r2epfsf.

Cyclic nucleotide-gated (CNG) ion channels play pivotal roles in sensory transduction by retinal photoreceptors and olfactory neurons. The elapid snake toxins pseudechetoxin (PsTx) and pseudecin (Pdc) are the only known protein blockers of CNG channels. These toxins belong to a cysteine-rich secretory protein (CRISP) family containing an N-terminal pathogenesis-related proteins of group 1 (PR-1) domain and a C-terminal cysteine-rich domain (CRD). PsTx and Pdc are highly homologous proteins, but their blocking affinities on CNG channels are different: PsTx blocks both the olfactory and retinal channels with ~15–30-fold higher affinity than Pdc. To gain further insights into their structure and function, the crystal structures of PsTx, Pdc and Zn^{2+}-bound Pdc were determined. The structures revealed that most of the amino-acid-residue differences between PsTx and Pdc are located around the concave surface formed between the PR-1 domain and the CRD, suggesting that the concave surface is functionally important for CNG-channel binding and inhibition. A structural comparison in the presence and absence of Zn^{2+} ion demonstrated that the concave surface can open and close owing to movement of the CRD upon Zn^{2+} binding. The data suggest that PsTx and Pdc occlude the pore entrance and that the dynamic motion of the concave surface facilitates interaction with the CNG channels.

1. Introduction

Cysteine-rich secretory proteins (CRISPs) are single-chain secreted proteins with molecular weights of 20–30 kDa which are characterized by a high cysteine content, especially in their C-terminal third (Yamazaki & Morita, 2004; Roberts *et al.*, 2006). The first described CRISP was protein D/E (also known as acidic epididymal glycoprotein, sperm coating protein and CRISP-1) from rat epididymis (Cameo & Blaquier, 1976; Brooks *et al.*, 1986). With the discovery of testis-specific protein 1 (Tpx-1, CRISP-2; Hardy *et al.*, 1988; Kasahara *et al.*, 1989) and specific granule protein of 28 kDa (SGP28, CRISP-3; Haendler *et al.*, 1993; Kjeldsen *et al.*, 1996), four CRISPs (CRISP-1–CRISP-4) have now been identified in mammalian tissues. Furthermore, it has also been shown that CRISPs are widely distributed in non-mammalian species, including *Xenopus* (Olson *et al.*, 2001), *Caenorhabditis elegans* (Ookuma *et al.*, 2003) and the venoms of lizards (Nobile *et al.*, 1994, 1996; Morrissette *et al.*, 1995), cone snails (Milne *et al.*, 2003; Hansson *et al.*, 2006) and snakes (Yamazaki & Morita, 2004, 2007). Although clear evidence for either function or target

molecules is lacking for most of the CRISPs, including endogenous CRISPs, recent evidence has emerged suggesting that some exogenous CRISPs derived from venomous snakes may function as ion-channel blockers (Nobile *et al.*, 1994, 1996; Brown *et al.*, 1999, 2003; Yamazaki, Brown *et al.*, 2002; Yamazaki, Koike *et al.*, 2002; Wang *et al.*, 2005).

Cyclic nucleotide-gated ion channels (CNG channels) are nonselective cation channels opened by the binding of cGMP and cAMP (Kaupp & Seifert, 2002; Brown *et al.*, 2006; Craven & Zagotta, 2006). CNG channels are expressed in the sensory epithelium of the visual and olfactory systems, where they play crucial roles in sensory transduction in retinal photoreceptors and olfactory neurons. Pseudechetoxin (PsTx) and pseudecin (Pdc), CRISPs derived from the venoms of Australian elapid snakes, are the only known protein blockers of CNG channels (Brown *et al.*, 1999; Yamazaki, Brown *et al.*, 2002). PsTx has recently been shown to directly bind to the pore-turret region of CNG channels (Brown *et al.*, 2003). Both PsTx and Pdc are highly basic proteins (their predicted pI is ∼10) and their primary structures are quite similar (differing at only seven residues; 97% identity; Fig. 1); surprisingly, however, there are large differences in their affinities for CNG channels (Yamazaki, Brown *et al.*, 2002). PsTx blocks olfactory and retinal CNG channels (CNGA2 and CNGA1, respectively) with a ∼15–30-fold higher affinity than Pdc (Yamazaki, Brown *et al.*, 2002). By understanding the structural basis for this affinity difference, we hope to provide mechanistic insights into the binding mode used to target the ion channels.

Here, we report the crystal structures of PsTx and Pdc determined at 2.25 and 1.90 Å resolution, respectively. The tertiary structures of PsTx and Pdc are quite similar to each other and also resemble those of other known CRISPs, such as triflin (Shikamoto *et al.*, 2005), stecrisp (Guo *et al.*, 2005) and natrin (Wang *et al.*, 2005, 2006), but the domain orientation of the cysteine-rich domain (CRD) against the pathogenesis-related proteins of group 1 (PR-1) domain is significantly different from those of other CRISPs. By solving the crystal structures in the presence and absence of Zn^{2+}, we have also demonstrated that the concave surface formed between the PR-1 domain and the CRD expands upon Zn^{2+} binding. Our data strongly suggest that the specificity and affinity of ion channel-blocking CRISPs are gained by cooperation between the PR-1 domain and the CRD, providing novel insight into the structure and function of CRISP-family proteins.

2. Materials and methods

2.1. Purification, crystallization and X-ray data collection

PsTx and Pdc were purified from the venoms of *Pseudecis australis* and *P. porphyriacus*, respectively, as described previously (Brown *et al.*, 1999; Yamazaki, Brown *et al.*, 2002).

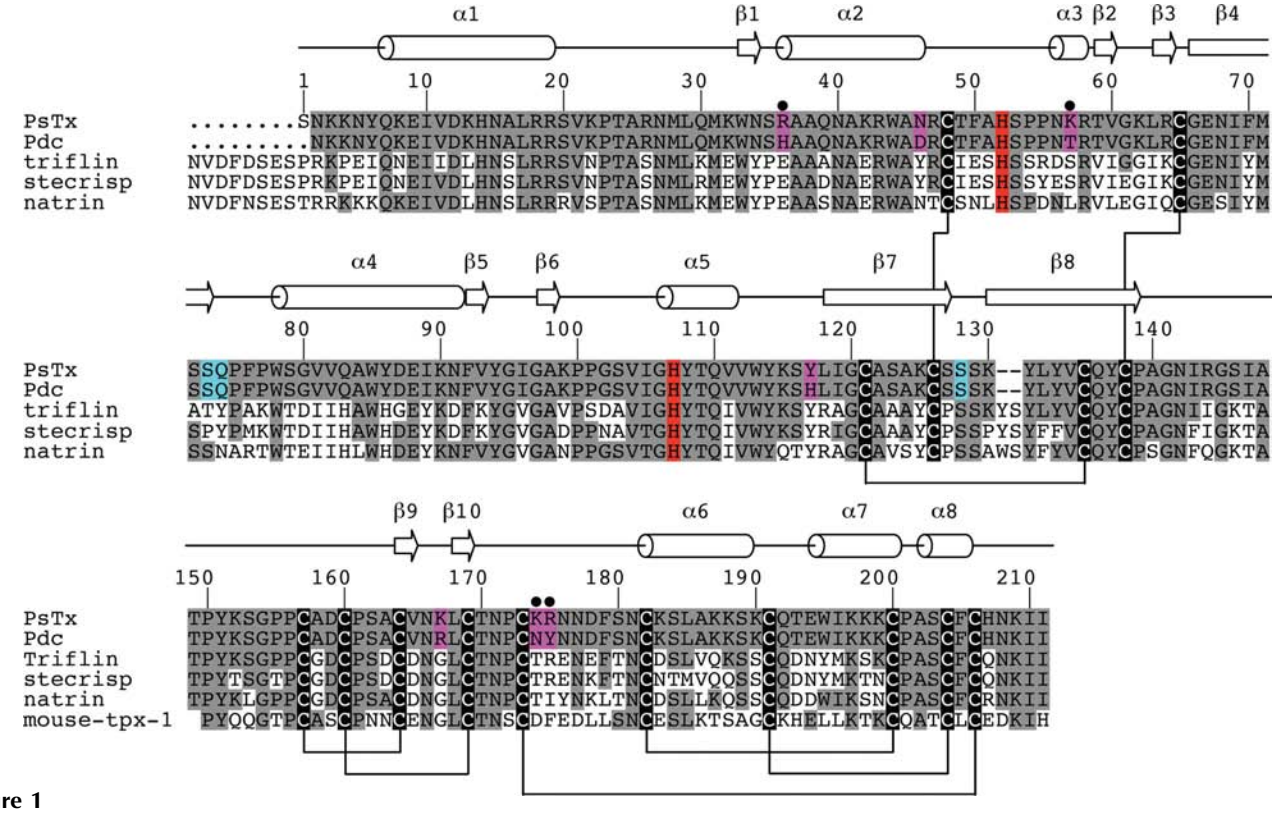

Figure 1
Sequence alignment of known structures of snake-venom CRISP-family proteins. Identical residues are shaded in grey. The residues involved in divalent-ion binding and Na^{+} binding are highlighted in red and in blue, respectively. All cysteine residues are shown as inverse characters and residues involved in disulfide bonds are connected by lines. The locations of the regular secondary-structure elements identified in PsTx are depicted at the top (α-helices and β-strands). The numbering for PsTx is indicated above the sequence. The seven different residues between PsTx and Pdc are shown in pink and the residues important for CNG-channel blockage are marked with dots.

Table 1
Data-collection and refinement statistics.

	PsTx	Pdc	Zn-Pdc
Data collection			
Space group	$P2_12_12_1$	$P2_12_12_1$	$P2_12_12_1$
Unit-cell parameters (Å)	a = 60.3, b = 61.6, c = 251.7	a = 60.7, b = 61.7, c = 251.2	a = 60.1, b = 62.3, c = 246.9
Resolution (Å)	50–2.25 (2.33–2.25)	50–1.90 (1.97–1.90)	50–2.3 (2.38–2.30)
R_{merge}	0.074 (0.253)	0.109 (0.315)	0.088 (0.394)
$I/\sigma(I)$	6.1 (3.5)	4.7 (2.1)	10.7 (3.8)
Completeness (%)	92.6 (72.2)	98.5 (100.0)	99.4 (95.2)
Redundancy	6.7 (6.1)	6.2 (7.2)	6.9 (5.9)
Refinement			
Resolution (Å)	48.97–2.25	43.27–1.90	38.72–2.30
No. of reflections	40102	70584	39944
R_{work}/R_{free}	0.203/0.259	0.206/0.258	0.219/0.277
No. of atoms			
Protein	6544	6514	6496
Ligand/ion	28	103	8
Water	446	721	196
B factors (Å^2)			
Protein	36.2	25.5	35.6
Ligand/ions	43.1	35.1	39.6
Waters	36.9	37.0	29.6
R.m.s. deviations			
Bond lengths (Å)	0.011	0.009	0.009
Bond angles (°)	1.263	1.173	1.140

Crystallization and X-ray data collection for PsTx and Pdc were conducted as reported by Suzuki *et al.* (2005). Briefly, the purified PsTx and Pdc were crystallized by the sitting-drop vapour-diffusion method at 293 K. Rod-shaped crystals of Pdc were obtained after a week by mixing 1 µl protein solution (10 mg ml^{-1} protein in 50 m*M* Tris–HCl buffer pH 8.0 containing 0.15 *M* NaCl) and an equal volume of reservoir solution (3.6 *M* sodium formate and 10% glycerol in the same buffer) and equilibrating against 50 µl reservoir solution. Similarly, rod-shaped crystals of PsTx were obtained under the same conditions but the reservoir solution was diluted 1.5-fold with buffer. X-ray diffraction data collection for Pdc was performed at 100 K on beamline BL6B, PF, Tsukuba, Japan. The diffraction was measured at 1.90 Å resolution and the data were processed using the program *CrystalClear* (Rigaku). Diffraction data collection for PsTx was performed at 100 K on beamline NW12, PF-AR, Tsukuba, Japan. The diffraction data were collected to 2.25 Å resolution and were processed using the program *HKL*-2000 (Otwinowski & Minor, 1997).

The Zn^{2+}-bound Pdc crystals were obtained using the same conditions as for the native Pdc crystals, but with 3 m*M* Zn^{2+} acetate added to the precipitant solution. Crystals of Zn^{2+}-bound Pdc that resembled the native Pdc crystals were obtained. The X-ray diffraction experiment was performed on beamline NW12, PF-AR, Tsukuba, Japan and a data set was collected to 2.30 Å resolution and processed using the program *HKL*-2000 (Otwinowski & Minor, 1997). The data-processing statistics are tabulated in Table 1.

2.2. Structure determination

The structure of Pdc was determined by the molecular-replacement method with the program *MOLREP* (Vagin & Teplyakov, 2000) from the *CCP*4 suite (Collaborative Computational Project, Number 4, 1994). A search model for Pdc was constructed by homology modelling based on the coordinates of triflin (PDB code 1wvr; Shikamoto *et al.*, 2005) using *InsightII*2000 (Accelrys). After cycles of refinement with the program *REFMAC*5 (Murshudov *et al.*, 1997) from the *CCP*4 suite, electron density for residues 4–170, which correspond to the N-terminal PR-1 domain of triflin (Shikamoto *et al.*, 2005), was clearly visible, although that for the ∼40 C-terminal residues was ambiguous. Models of the C-terminal domains were then reconstructed using the program *XTALVIEW* (McRee, 1999) and refined using *REFMAC*5. When further refinement of the model using *REFMAC*5 and *XTALVIEW* reduced the R factor to ∼0.25, water molecules and other metal ions and ligands were added to the model for further refinement. Finally, the R and R_{free} factors fell to 0.206 and 0.258, respectively; the model contained four Pdc molecules (residues 4–210), 721 water molecules, four sodium ions, 22 formate ions and six glycerol molecules. The structure of PsTx was determined using the coordinates of Pdc as a starting model and was refined using *REFMAC*5. The R and R_{free} factors of the final PsTx model were 0.203 and 0.259, respectively. The model contained four PsTx molecules (residues 4–211), 446 water molecules, four sodium ions, six formate ions and a glycerol molecule. The final model of Zn^{2+}-bound Pdc also contained four Pdc molecules (residues 4–210), 196 water molecules, five Zn^{2+} ions and three Na^{+} ions, with R and R_{free} factors of 0.219 and 0.277, respectively. At the final stage, the models were validated using the program *PROCHECK* (Laskowski *et al.*, 1993). The refinement statistics are summarized in Table 1. The figures were produced using the programs *MOLSCRIPT* (Kraulis, 1991), *Raster3D* (Merritt & Bacon, 1997), *PyMOL* (DeLano, 2005) and *APBS* (Baker *et al.*, 2001).

2.3. Chemical synthesis of the PsTx cysteine-rich domain

A peptide consisting of the final 40 amino acids of PsTx (Pro172–Ile211), comprising the entire CRD, was synthesized on an Applied Biosystems 433A synthesizer and was partially purified by RP-HPLC as described previously (Pokidysheva *et al.*, 2004). The partially purified peptide was then oxidized by the addition of a mixture of oxidized and reduced glutathione and was characterized by electrospray ionization quadrupole time-of-flight mass spectroscopy. The molecular weight of the reduced peptide was 4631.5 Da prior to oxidation and 4625.5 Da following oxidation, suggesting the formation of three disulfide bonds. The oxidized PsTx-CRD was then

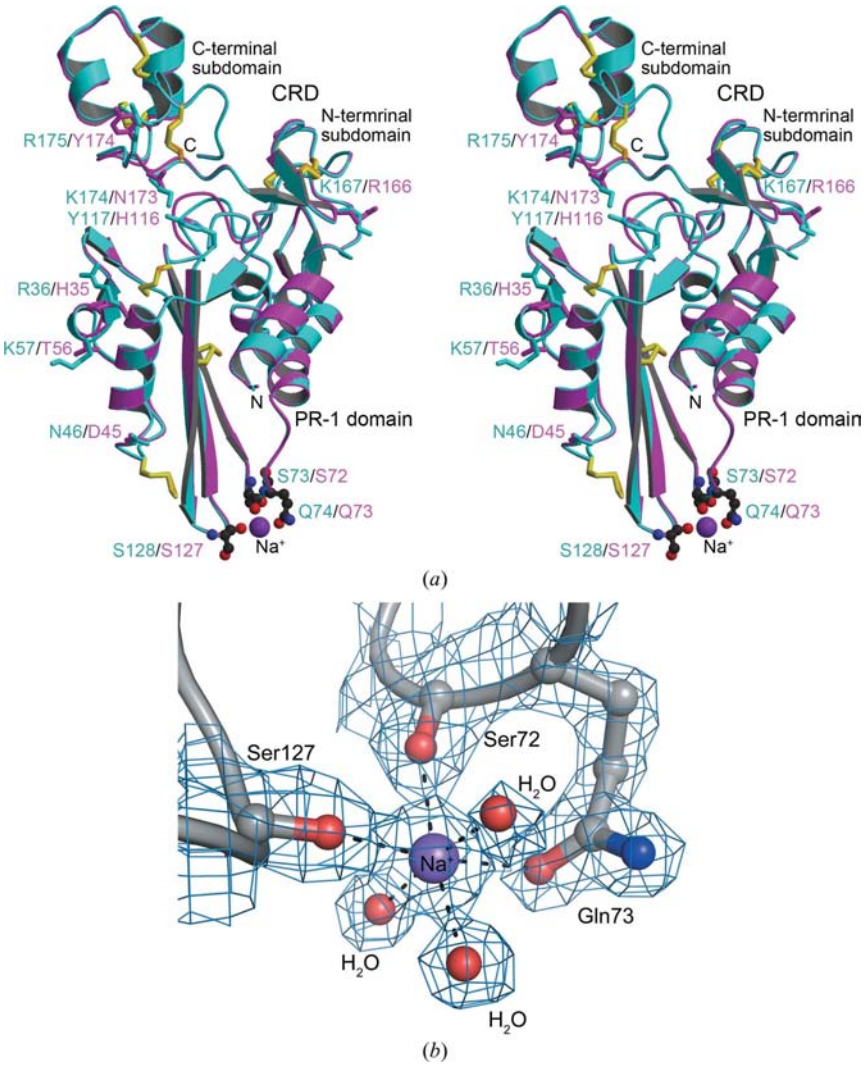

Figure 2
(*a*) Stereoview of the structural comparison between PsTx and Pdc. Ribbon models of PsTx and Pdc are shown in cyan and magenta, respectively. Amino-acid residues that differ between PsTx and Pdc are indicated by side chains and are labelled. The Na^+ ion-binding site at the bottom is shown with the side chains of the coordinated residues (labelled) and the bound Na^+ ion as a purple sphere. (*b*) A close-up view of the Na^+ ion-coordination geometries in Pdc with $2F_o - F_c$ electron-density map contoured at 1.5σ.

purified by preparative reverse-phase HPLC on a Vydac C18 column using an acetonitrile gradient containing 0.1% trifluoroacetic acid. The oxidized product eluted as a single peak, suggesting proper protein folding and correct disulfide bonding.

2.4. Whole-cell patch-clamp recording of CNGA2 currents from transfected HEK-293 cells

HEK-293 cells were grown and transfected with a plasmid encoding CNGA2 as previously described (Brown *et al.*, 2003). Whole-cell patch-clamp recordings were made using an Axopatch 200A amplifier as described previously (Brown *et al.*, 2003).

3. Results and discussion

3.1. Overall structures of PsTx and Pdc and comparison with other snake-venom CRISPs

The crystal structures of PsTx, Pdc and Zn-Pdc were determined and refined at 2.25, 1.90 and 2.30 Å resolution, respectively (Table 1, Fig. 2*a*). As expected for isomorphous crystals, the crystal structures of PsTx and Pdc are very similar to each other and contain four molecules in the asymmetric unit. The average root-mean-square (r.m.s.) differences in the C^{α}-atom positions between each pair of molecules is 0.71 Å in PsTx and 0.83 Å in Pdc. The major differences in their backbone structures are mainly confined to the flexible and solvent-exposed loops (residues 142–146 and 205–207 in PsTx and 141–145 and 205–207 in Pdc), in which the electron densities were relatively weak. Furthermore, the structures of PsTx and Pdc are very similar to each other, with an r.m.s. difference of C^{α}-atom positions of below 1.00 Å, as might be expected from their highly homologous amino-acid sequences (97% identity), as shown in Fig. 1. The overall features and secondary-structure elements of the proteins resemble those of the known crystal structures of snake-venom CRISP members, including triflin (Shikamoto *et al.*, 2005), stecrisp (Guo *et al.*, 2005) and natrin (Wang *et al.*, 2005, 2006) (Fig. 3*a*), reflecting the high degree of identity in their amino-acid sequences (Fig. 1). The proteins can be divided into two domains, as shown previously for triflin (Shikamoto *et al.*, 2005). One domain comprises the N-terminal 153 residues of PsTx (or 152 residues of Pdc as PsTx has one additional residue at the N-terminus, as shown in Fig. 1), which form a globular domain that includes an α-β-α sandwich core and has a fold similar to the pathogenesis-related proteins of group 1 (PR-1) proteins, *e.g.* P14a (Fernandez *et al.*, 1997) and GAPR1 (Serrano *et al.*, 2004), and the antigen 5 proteins, *e.g.* Ves v 5 (Henriksen *et al.*, 2001). The subsequent residues Gly-Pro-Pro form a short linker, as described in the structure of triflin (Shikamoto *et al.*, 2005). The succeeding cysteine-rich domain (CRD) starts with Cys157 and ends at the terminal residue Ile211 of PsTx (Cys156–Ile210 in Pdc). This CRD forms an unusually elongated shape that spans about 38 Å (Fig. 2*a*) and can be subdivided into N- and C-terminal subdomains (Cys157–Cys169 and Thr170–Ile211 in PsTx), as previously described in the structure of triflin (Shikamoto *et al.*, 2005). The N-terminal subdomain forms a compact fold with two short β-strands and two disulfide bonds. This

subdomain contacts the PR-1 domain *via* two hydrogen bonds, but makes no contact with the C-terminal subdomain. Therefore, the N-terminal subdomain together with the short linker region might be part of the PR-1 domain. The C-terminal subdomain is folded into three α-helices stabilized by three disulfide bonds. This fold is similar to those of the small peptide toxins from sea anemones such as ShK (Tudor *et al.*, 1996) and BgK (Dauplais *et al.*, 1997), in which all three disulfide bonds are conserved despite low sequence similarity (Guo *et al.*, 2005). The C-terminal subdomain does not interact with either the PR-1 domain or the N-terminal subdomain, apart from the C-terminal carboxyl group, which hydrogen bonds to the side chains of Tyr114 and Lys115 of the PR-1 domain. These data suggest that the C-terminal subdomain can move independently relative to the rest of the molecule. Rotations around certain covalent bonds in the backbone chain from Cys169 to Asn171 might cause domain movement and the interactions involving the C-terminal carboxyl group can be maintained because they are located in the proximity of the rotation axis. This is commonly observed in Pdc and triflin (Shikamoto *et al.*, 2005) and may also occur in the other family proteins stecrisp (Guo *et al.*, 2005) and natrin (Wang *et al.*, 2005, 2006). Fig. 3(*a*) shows a superposition of the known CRISPs. When only the PR-1 domain is superposed, changes or movements of the CRD are visible relative to the PR-1 domain. Such domain movement is also observed between Pdc and Zn-Pdc (Figs. 3*b* and 3*c*), suggesting a structural change upon Zn^{2+} binding.

3.2. Cation-binding sites

The conserved His residues shown in Fig. 1 (His52 and His107 in PsTx) form a putative divalent cation-binding site in snake-venom CRISPs. The biological function of this site is not known, but the corresponding sites of other CRISP and PR-1-family proteins have been extensively discussed as Zn^{2+}-binding sites and in relation to the activity (Fernandez *et al.*, 1997; Szyperski *et al.*,

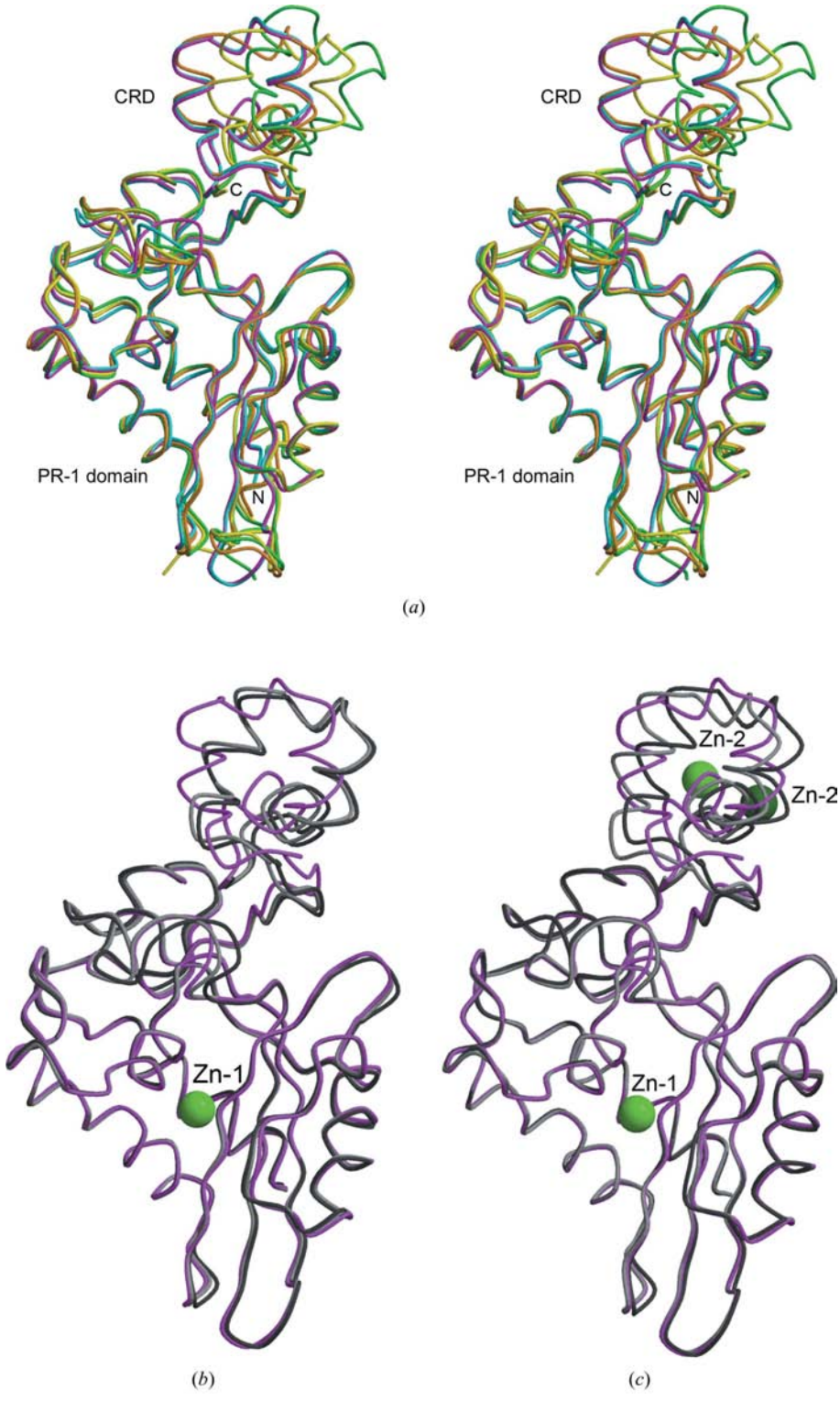

Figure 3
Domain movement and Zn^{2+}-binding sites. (*a*) Stereoview of the superposition of snake-venom CRISP-family proteins (PsTx, cyan; Pdc, magenta; triflin, green; stecrisp, yellow; natrin, orange). When the only PR-1 domains are superposed, changes or movement of the CRD domains are visible relative to the PR-1 domain. (*b*) Pdc (magenta) is superposed with Zn-Pdc (molecule *B*, light grey; molecule *D*, dark grey) and Zn-1 is shown as a green sphere. (*c*) As (*b*) but superposed with Zn-Pdc (molecule *A*, light grey; molecule *C*, dark grey). The Zn-2 bound to molecule *A* and to molecule *C* is shown as a green and a dark green sphere, respectively.

1998; Milne *et al.*, 2003). We previously found a Cd^{2+} ion in the corresponding binding site of triflin. *In vivo*, this Cd^{2+} may be replaced by a Zn^{2+} ion. The present structures of Zn-Pdc revealed two bound Zn^{2+} ions: Zn-1 in the cation-binding site and Zn-2 between molecules *A* and *C* (Figs. 3*b* and 3*c*). Figs. 3(*d*) and 3(*e*) show the coordination geometry with electron densities. In the Zn-1 binding site, the $N^{\varepsilon 2}$ atoms of His51 and His106 coordinate to the Zn^{2+} ion. Electron density for a water molecule is visible at the third coordination position but not at the fourth coordination position. The carboxyl O atoms of Glu66 and Glu87 form hydrogen bonds to the $N^{\delta 1}$ atoms of His51 and His106, respectively. These hydrogen bonds are conserved even in the unbound states of PsTx and Pdc, allowing the His residues to face each other and to adopt the proper conformation to bind a divalent cation. His51, His106, Glu66 and Glu87 are conserved and may assist in forming this conformation by hydrogen bonding, as previously described for triflin (Shikamoto *et al.*, 2005). In the Zn-2 binding site, His206 $N^{\varepsilon 2}$ of molecule *A* and His206 $N^{\delta 1}$ of molecule *C* coordinate to the Zn^{2+} ion, and two water molecules occupy the third and fourth coordination sites (Fig. 3*e*). Since the His206 residue is in the CRD, it appears that Zn-2 directly influences the domain movement of CRD. We consider the second zinc-binding site, Zn-2, to be an artifact of crystalline lattice formation and it causes some structural deformation, as the CRD moves slightly (molecule *A*) or largely (molecule *C*) relative to the PR-1 domain dependent on crystal packing. In contrast, molecules *B* and *D* have no Zn^{2+} ions associated with the CRD (Fig. 3*b*), so that a similar extent of rotation in the clockwise direction is likely to occur upon Zn^{2+} binding in the Zn-1 site.

We also found a putative Na^+ ion-binding site in both PsTx and Pdc, as shown in Fig. 2(*a*). Our assignment is based on electron densities (Fig. 2*b*) and the observed coordination geometries. The Na^+ ion is coordinated by the backbone carboxyl O atoms of Ser73 (Ser72 in Pdc) and Ser128 (Ser127 in Pdc), the side-chain O atom of Gln74 (Gln73 in Pdc) and three solvent O atoms in PsTx (and in Pdc). In the Na^+ ion-binding site in the Zn-Pdc crystal, the Na^+ ion is replaced by a water molecule in molecule *B*. This Na^+-ion binding has not been found in other snake-venom CRISPs, probably because Gln74 is replaced by other amino-acid residues. The above three residues are located at the tips of two loops, as shown at the bottom of Fig. 2(*a*). The role of this Na^+-ion binding has not been reported, but it may contribute to stabilization of the local loop structure.

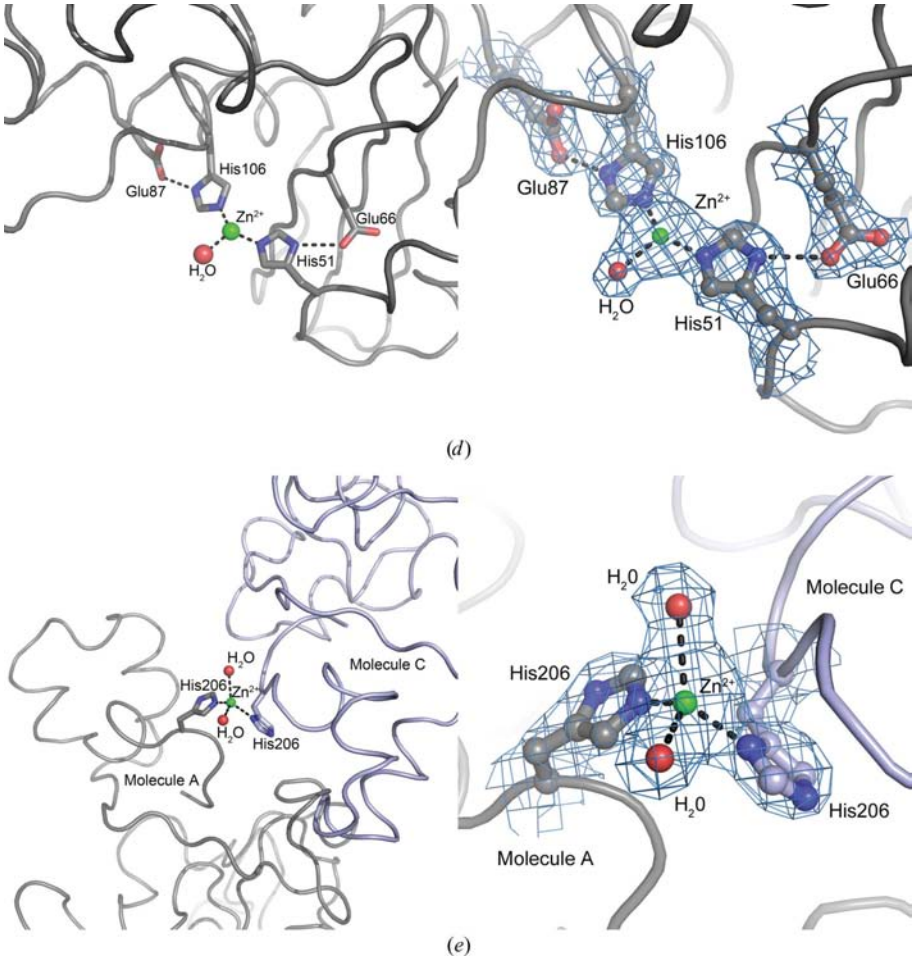

Figure 3 (continued)
(*d*) Zn-1 coordination (left) and a close-up view with $2F_o - F_c$ electron-density map contoured at 1.0 in Zn-Pdc (right). (*e*) Zn-2 coordination between molecules *A* and *C* in Zn-Pdc (left) and a close-up view with $2F_o - F_c$ electron-density map (right).

3.3. Implications of the interaction with the pore turret of CNGA2

Although the crystal structure of the CNG channel has not been solved, the structures of the KcsA (Zhou & MacKinnon, 2003), KvAP (Jiang *et al.*, 2003) and Kv1.2 (Long *et al.*, 2005) channels have been determined and have revealed that the pore turret forms a loop that connects the outer helix (S5) and the pore helix. In contrast, the crystal structure of NaK (Shi *et al.*, 2006) has only three residues in this region, which appear to be just a linker rather than a turret. To identify the turret region of the CNG channel, a sequence alignment was performed. Fig. 4 shows a structure-based sequence alignment of the turret region, including the neighbouring residues, on which the corresponding residues of CNGA2 were aligned manually. This alignment suggests that the turret sequence of CNGA2 starts at Thr308, because five continuous hydrophobic residues flanked by a conserved acidic residue are assigned as the C-terminus of the outer helix. These hydrophobic residues

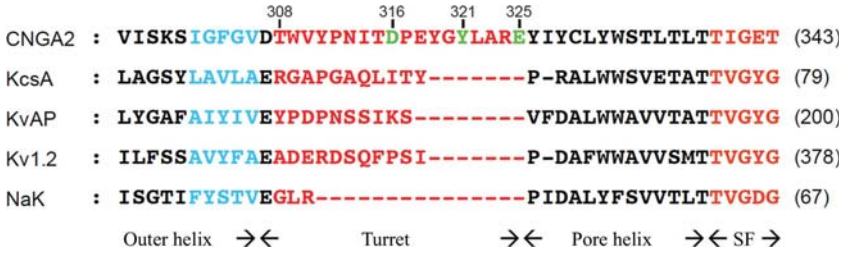

Figure 4
Sequence comparison of CNG with K^+ and NaK channels. The amino-acid residues of CNGA2, containing the pore turret, are compared with those of KcsA, KvAP, Kv1.2 and NaK, which have known structures. The turret sequence is shown in red; the outer helix and the pore helix are located on the left and right sides of the turret region, respectively. Hydrophobic residues with some homology are shown in blue. The SF (selectivity filter) sequence is shown in orange. Asp316, Tyr321 and Glu325 in CNGA2, shown in green, are important residues for the interaction with PsTx.

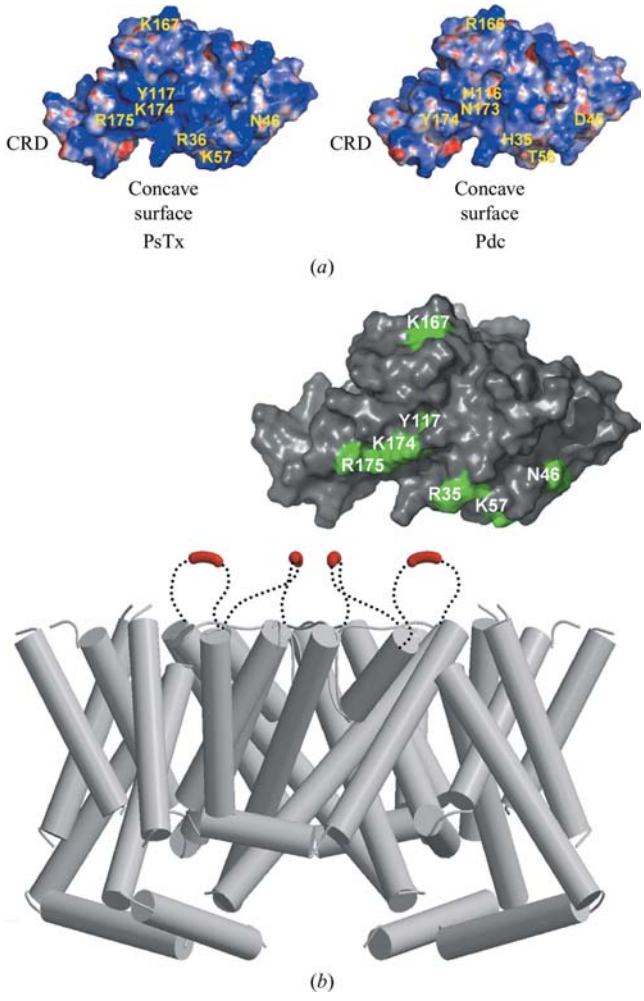

Figure 5
Interaction between PsTx and the CNG pore turret. (*a*) Surface-potential model of PsTx compared with that of Pdc. Amino-acid residues that differ between PsTx and Pdc are indicated by labels. (*b*) Docking model of the interaction between the CNG channel and PsTx. Helical models (cylinders) in the CNG channel were prepared by using those of the Kv1.2 channel and the turret regions are shown by dotted lines, in which acidic residues are shown in red. Thus, this CNG-channel model is likely to correspond to the homotetrameric CNGA2 model. The concave surface of PsTx is shown at the bottom for the interaction with the pore turret, where only the different amino-acid residues between PsTx and Pdc are highlighted in green, with labels for clarity.

are well conserved and are involved in inter-helix interactions with the pore and/or S6 helices. Thus, the CNGA2 turret region is predicted to be 18 residues in length and to contain Asp316, Tyr321 and Glu325, which are known to be important for high-affinity inhibition by PsTx (Brown *et al.*, 2003). This extended turret region of CNGA2 is not conserved in the other ion channels and is longer than the turret regions of other ion channels, which are typically ∼10 residues in length (Fig. 4). A longer more flexible turret loop may provide unique opportunities and mechanisms for specific high-affinity interactions. Surprisingly, PsTx and Pdc are the only protein ligands so far discovered for the CNG pore turret. As previously mentioned, the crystal structures of these two proteins are very similar to each other. Despite their high structural similarity, PsTx blocked olfactory CNG-channel (CNGA2) currents with 30-fold higher affinity than Pdc (K_d = 15 n*M* *versus* 460 n*M*) and also blocked the rod-type channel (CNGA1) with 15-fold higher affinity (K_d = 70 n*M* *versus* 1000 n*M*) (Yamazaki, Brown *et al.*, 2002), suggesting that the affinity difference between PsTx and Pdc is a consequence of the seven amino-acid differences in the primary sequence. Most of these differences (see Fig. 2*a*) are located on the concave surface. We hypothesize that the substitution of four basic residues in PsTx, Arg36 (His35 in Pdc), Lys57 (Thr56 in Pdc), Lys174 (Asn173 in Pdc) and Arg175 (Tyr174 in Pdc), which forms a more positively charged concave surface in PsTx, may be responsible for the higher affinity of PsTx compared with Pdc (Fig. 5*a*). These toxin residues could thus be considered to interact with the acidic residues of Asp316 and Glu325 of the CNGA2 turret (see Fig. 4), which are known to be important for high-affinity PsTx binding.

In addition to electrostatic interactions, hydrophobic interactions may be considered as another binding mode. Conserved hydrophobic residues in the CRD in the snake-venom CRISP-family proteins are exposed on the molecular surface at the edge of the concave surface (Shikamoto *et al.*, 2005). These hydrophobic residues may interact with hydrophobic residues in the pore turret, contributing to stabilization of the binding. Tyr321 in the turret of CNGA2 may be responsible for the higher affinity of PsTx compared with Pdc.

Compared with most other peptide toxins, the CRISP-family proteins are considerably larger molecules, with a concave surface about 35 Å in length. It has been suggested that PsTx and Pdc may occlude the external vestibule formed by the four pore turrets in a manner in which the concave surface binds one of the turrets and the CRD covers the pore entrance formed by the four pore turrets (Fig. 5*b*). This is consistent with previous biochemical results, in which only one molecule of PsTx was required for the inhibition of CNG channels (Brown *et al.*, 1999). If this is true, then this interaction mechanism is in stark contrast to those employed by most peptide toxins. For example, in the NMR structure of the

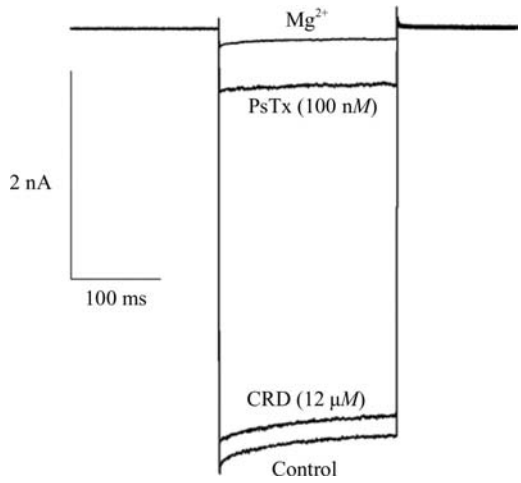

Figure 6
The isolated CRD of PsTx is not an effective blocker of CNGA2. The currents elicited by −50 mV pulses were recorded from HEK-293 cells expressing CNGA2. PsTx (100 n*M*) or its isolated CRD (12 μ*M*) was bath applied. The application of Mg^{2+} blocks >98% of the current through CNGA2, indicating the 'leak' current through the seal resistance. This trace is representative of results from four cells.

kalitoxin (38 amino-acid residues)–KcsA–Kv1.3 (chimeric K^+ channel) complex, the side chain of Lys27 is inserted deeply into the selectivity filter and plugs the K^+-channel pore (Lange *et al.*, 2006). It was recently reported that the cysteine-rich domain of recombinant mouse Tpx-1 is responsible for the inhibition of the ryanodine receptor (Gibbs *et al.*, 2006), suggesting that the cysteine-rich domain itself possesses the ion-channel blocking activity. Furthermore, molecular-docking simulations with natrin suggested that the CRD alone is sufficient for the inhibition of Kv1.3, although this has not been tested directly (Wang *et al.*, 2006).

To test directly the inhibitory ability of the PsTx CRD, we chemically synthesized the C-terminal subdomain of the PsTx CRD starting at Pro172. When applied to HEK-293 cells expressing CNGA2 channels, the purified CRD blocked little if any of the current, even at a concentration of >10 μ*M* (3 ± 2% inhibition; $n = 5$). In contrast, the full-length PsTx was quite effective even at a 100-fold lower concentration (89 ± 5% inhibition; $n = 4$; Fig. 6). Therefore, it appears that the CRD of PsTx is not sufficient for high-affinity inhibition of CNG channels, indicating that other contacts with the concave surface may be required. As described above, the CRD has a similar fold to those of BgK and ShK, which are small peptidic blockers of voltage-gated K^+-channels. These blockers have been shown to interact with the selectivity filter and the vestibule of the target channels, rather than the pore turret (Rauer *et al.*, 1999; Lanigan *et al.*, 2002). The interaction site of the blockers with channels has been localized to the C-terminal end of the molecule (corresponding to the C-terminal end of the CRD of PsTx). These differences suggest that the interaction mode between small peptidic blockers with the CRD-like structure and their target channels is distinct from that between PsTx and CNG channels.

Snake-venom CRISP-family proteins consist of PR-1 and cysteine-rich domains and the role of the PR-1 domain has not been clearly defined. As mentioned above, we suggested that the concave surface formed by the PR-1 and cysteine-rich domains is involved in interaction with ion channels. Previously, we described the opening and closing of the concave surface based on the domain movement (Shikamoto *et al.*, 2005), which might provide a basis for induced fitting. The present observation in Zn-Pdc (Fig. 3*b*) suggests domain movement upon Zn^{2+} binding, which might be a possible role of the Zn^{2+} ion or divalent cations. Thus, a wider interaction area and the opening and closing of the concave surface are apparently advantageous for binding affinity and specificity. We suggest that the high specificity and affinity of the snake-venom CRISP-family proteins as ion-channel blockers are gained by cooperation between the cysteine-rich and PR-1 domains and that the pore turret of CNGA2 is a potential target site for PsTx and Pdc.

The authors would like to thank Dr Hans Peter Bächinger (Oregon Health and Science University, Portland, Oregon, USA) for synthesis of the PsTx CRD peptide. We also thank Dr Yasuo Shikamoto (National Institute of Advanced Industrial Science and Technology, Tsukuba, Japan) and Katsunori Horii (NEC Soft Ltd, Tokyo, Japan) for their helpful suggestions during the crystal structure analyses. This research was supported by Scientific Research Grants-in-Aid (TM), by Special Coordination Funds for Promoting Science and Technology (HM) from the Ministry of Education, Science, Sports and Culture of Japan and by grant MH67094 (RLB) from NIMH.

References

Baker, N. A., Sept, D., Joseph, S., Holst, M. J. & McCammon, J. A. (2001). *Proc. Natl Acad. Sci. USA*, **98**, 10037–10041.
Brooks, D. E., Means, A. R., Wright, E. J., Singh, S. P. & Tiver, K. K. (1986). *Eur. J. Biochem.* **161**, 13–18.
Brown, R. L., Haley, T. L., West, K. A. & Crabb, J. W. (1999). *Proc. Natl Acad. Sci. USA*, **96**, 754–759.
Brown, R. L., Lynch, L. L., Haley, T. L. & Arsanjani, R. (2003). *J. Gen. Physiol.* **122**, 749–760.
Brown, R. L., Strassmaier, T., Brady, J. D. & Karpen, J. W. (2006). *Curr. Pharm. Des.* **12**, 3597–3613.
Cameo, M. S. & Blaquier, J. A. (1976). *J. Endocrinol.* **69**, 47–55.
Collaborative Computational Project, Number 4 (1994). *Acta Cryst.* D**50**, 760–763.
Craven, K. B. & Zagotta, W. N. (2006). *Annu. Rev. Physiol.* **68**, 375–401.
Dauplais, M., Lecoq, A., Song, J., Cotton, J., Jamin, N., Gilquin, B., Roumestand, C., Vita, C., de Medeiros, C. L., Rowan, E. G., Harvey, A. L. & Menez, A. (1997). *J. Biol. Chem.* **272**, 4302–4309.
DeLano, W. L. (2005). *Drug Discov. Today*, **10**, 213–217.
Fernandez, C., Szyperski, T., Bruyere, T., Ramage, P., Mosinger, E. & Wuthrich, K. (1997). *J. Mol. Biol.* **266**, 576–593.
Gibbs, G. M., Scanlon, M. J., Swarbrick, J., Curtis, S., Gallant, E., Dulhunty, A. F. & O'Bryan, M. K. (2006). *J. Biol. Chem.* **281**, 4156–4163.
Guo, M., Teng, M., Niu, L., Liu, Q., Huang, Q. & Hao, Q. (2005). *J. Biol. Chem.* **280**, 12405–12412.
Haendler, B., Kratzschmar, J., Theuring, F. & Schleuning, W. D. (1993). *Endocrinology*, **133**, 192–198.
Hansson, K., Thamlitz, A. M., Furie, B., Furie, B. C. & Stenflo, J. (2006). *Biochemistry*, **45**, 12828–12839.

Hardy, D. M., Huang, T. T. Jr, Driscoll, W. J., Tung, K. K. & Wild, G. C. (1988). *Biol. Reprod.* **38**, 423–437.
Henriksen, A., King, T. P., Mirza, O., Monsalve, R. I., Meno, K., Ipsen, H., Larsen, J. N., Gajhede, M. & Spangfort, M. D. (2001). *Proteins*, **45**, 438–448.
Jiang, Y., Lee, A., Chen, J., Ruta, V., Cadene, M., Chait, B. T. & MacKinnon, R. (2003). *Nature (London)*, **423**, 33–41.
Kasahara, M., Gutknecht, J., Brew, K., Spurr, N. & Goodfellow, P. N. (1989). *Genomics*, **5**, 527–534.
Kaupp, U. B. & Seifert, R. (2002). *Physiol. Rev.* **82**, 769–824.
Kjeldsen, L., Cowland, J. B., Johnsen, A. H. & Borregaard, N. (1996). *FEBS Lett.* **380**, 246–250.
Kraulis, P. J. (1991). *J. Appl. Cryst.* **24**, 946–950.
Lange, A., Giller, K., Hornig, S., Martin-Eauclaire, M. F., Pongs, O., Becker, S. & Baldus, M. (2006). *Nature (London)*, **440**, 959–962.
Lanigan, M. D., Kalman, K., Lefievre, Y., Pennington, M. W., Chandy, K. G. & Norton, R. S. (2002). *Biochemistry*, **41**, 11963–11971.
Laskowski, R. A., MacArthur, M. W., Moss, D. S. & Thornton, J. M. (1993). *J. Appl. Cryst.* **26**, 283–291.
Long, S. B., Campbell, E. B. & MacKinnon, R. (2005). *Science*, **309**, 897–903.
McRee, D. E. (1999). *J. Struct. Biol.* **125**, 156–165.
Merritt, E. A. & Bacon, D. J. (1997). *Methods Enzymol.* **277**, 505–524.
Milne, T. J., Abbenante, G., Tyndall, J. D., Halliday, J. & Lewis, R. J. (2003). *J. Biol. Chem.* **278**, 31105–31110.
Morrissette, J., Kratzschmar, J., Haendler, B., el-Hayek, R., Mochca-Morales, J., Martin, B. M., Patel, J. R., Moss, R. L., Schleuning, W. D., Coronado, R. & Possani, L. D. (1995). *Biophys. J.* **68**, 2280–2288.
Murshudov, G. N., Vagin, A. A. & Dodson, E. J. (1997). *Acta Cryst.* D**53**, 240–255.
Nobile, M., Magnelli, V., Lagostena, L., Mochca-Morales, J., Possani, L. D. & Prestipino, G. (1994). *J. Membr. Biol.* **139**, 49–55.
Nobile, M., Noceti, F., Prestipino, G. & Possani, L. D. (1996). *Exp. Brain. Res.* **110**, 15–20.
Olson, J. H., Xiang, X., Ziegert, T., Kittelson, A., Rawls, A., Bieber, A. L. & Chandler, D. E. (2001). *Proc. Natl Acad. Sci. USA*, **98**, 11205–11210.
Ookuma, S., Fukuda, M. & Nishida, E. (2003). *Curr. Biol.* **13**, 427–431.
Otwinowski, Z. & Minor, W. (1997). *Methods Enzymol.* **276**, 307–326.
Pokidysheva, E., Milbradt, A. G., Meier, S., Renner, C., Haussinger, D., Bachinger, H. P., Moroder, L., Grzesiek, S., Holstein, T. W., Ozbek, S. & Engel, J. (2004). *J. Biol. Chem.* **279**, 30395–30401.
Rauer, H., Pennington, M., Cahalan, M. & Chandy, K. G. (1999). *J. Biol. Chem.* **274**, 21885–21892.
Roberts, K. P., Ensrud, K. M., Wooters, J. L., Nolan, M. A., Johnston, D. S. & Hamilton, D. W. (2006). *Mol. Cell. Endocrinol.* **250**, 122–127.
Serrano, R. L., Kuhn, A., Hendricks, A., Helms, J. B., Sinning, I. & Groves, M. R. (2004). *J. Mol. Biol.* **339**, 173–183.
Shi, N., Ye, S., Alam, A., Chen, L. & Jiang, Y. (2006). *Nature (London)*, **440**, 570–574.
Shikamoto, Y., Suto, K., Yamazaki, Y., Morita, T. & Mizuno, H. (2005). *J. Mol. Biol.* **350**, 735–743.
Suzuki, N., Yamazaki, Y., Fujimoto, Z., Morita, T. & Mizuno, H. (2005). *Acta Cryst.* F**61**, 750–752.
Szyperski, T., Fernandez, C., Mumenthaler, C. & Wuthrich, K. (1998). *Proc. Natl Acad. Sci. USA*, **95**, 2262–2266.
Tudor, J. E., Pallaghy, P. K., Pennington, M. W. & Norton, R. S. (1996). *Nature Struct. Biol.* **3**, 317–320.
Vagin, A. & Teplyakov, A. (2000). *Acta Cryst.* D**56**, 1622–1624.
Wang, F., Li, H., Liu, M. N., Song, H., Han, H. M., Wang, Q. L., Yin, C. C., Zhou, Y. C., Qi, Z., Shu, Y. Y., Lin, Z. J. & Jiang, T. (2006). *Biochem. Biophys. Res. Commun.* **351**, 443–448.
Wang, J., Shen, B., Guo, M., Lou, X., Duan, Y., Cheng, X. P., Teng, M., Niu, L., Liu, Q., Huang, Q. & Hao, Q. (2005). *Biochemistry*, **44**, 10145–10152.
Yamazaki, Y., Brown, R. L. & Morita, T. (2002). *Biochemistry*, **41**, 11331–11337.
Yamazaki, Y., Koike, H., Sugiyama, Y., Motoyoshi, K., Wada, T., Hishinuma, S., Mita, M. & Morita, T. (2002). *Eur. J. Biochem.* **269**, 2708–2715.
Yamazaki, Y. & Morita, T. (2004). *Toxicon*, **44**, 227–231.
Yamazaki, Y. & Morita, T. (2007). *Curr. Pharm. Des.* **13**, 2872–2886.
Zhou, Y. & MacKinnon, R. (2003). *J. Mol. Biol.* **333**, 965–975.